Chemical Physics Letters 494 (2010) 182–187

Contents lists available at ScienceDirect

Chemical Physics Letters

journal homepage: www.elsevier.com/locate/cplett

Phase transition and crossover behavior of colloidal fluids under confinement

Sudhir K. Singh [a], Jayant K. Singh [a,*], Sang Kyu Kwak [b], Goutam Deo [a]

[a] Department of Chemical Engineering, Indian Institute of Technology Kanpur, Kanpur 208016, India
[b] Division of Chemical and Biomolecular Engineering, School of Chemical and Biomedical Engineering, Nanyang Technological University, Singapore 637459, Singapore

ARTICLE INFO

Article history:
Received 17 April 2010
In final form 3 June 2010
Available online 8 June 2010

ABSTRACT

We report a molecular simulation study on the non-monotonic behavior of critical temperature, T_{cp}, of a confined Yukawa fluid. Close to the adhesive hard sphere (AHS) range of the surface–fluid interaction, T_{cp} monotonically increases with increasing surface–fluid interaction range. Subsequently, after a certain threshold value, depending on the surface interaction well depth, T_{cp} decreases monotonically with further increase in the surface interaction range. On the other hand, critical density and pressure show increasing monotonic trends with the surface interaction range. The crossover from 3D to 2D behavior for colloidal fluid in attractive pores is observed around a slit width of 14 molecular diameters for the studied system in this work.

1. Introduction

Colloidal suspensions are well-defined mesoscopic particles possessing linear dimensions ranging from 10 to 1000 nm and are receiving increasing attention amongst scientists. The colloidal particles, such as proteins, micelles, synthetic polymeric particles, etc., are significantly larger than the interacting ambient molecules, but small enough to show the random motion. Suspensions of these colloidal particles play an important role in biology, e.g. blood, but also many industrial products, such as paints, inks, food, detergents and cosmetics. Colloidal systems have been recognized as excellent model systems for various thermodynamical problems in statistical physics [1,2]. In addition, colloids are also useful for the investigation of non-bulk systems where geometrical constraints such as patterned walls, pores and channels have pronounced effects on the static and dynamical properties. Since such geometric confinements play an important role in many physical, biological and chemical processes, studies with colloidal suspensions may help to obtain a better understanding of several phenomena, e.g. transport of particles through cell membranes or catalytic reactions in zeolitic materials. Moreover, the effective interaction between the charged colloids or colloidal particle and ambient molecules or surfaces can be tailored by adding salt ions or smaller colloids of varying size and concentrations. The possibility of tailoring the effective interactions enriches the physics of the colloidal system compared to simple (atomic) fluids, and leads to a wide range of practical applications as well as fundamental interests.

On the basis of some intriguing experimental observations in aqueous suspensions of charged colloids [3,4] and subsequent theoretical prediction [5] on charged colloidal spheres it can be concluded that like-charged colloids, dispersed in an aqueous solvent, spontaneously demix into a colloid-dilute 'gas-like' phase and a colloid-dense 'liquid-like' phase. In further investigations Klapp et al. studied the structure formation of charged colloidal suspensions, in bulk and in slit pore geometry using theoretical and experimental techniques [6,7].

Anderson and Lekkerkerker [8] have indicated that colloids display fascinating phase transitions between fluid–fluid, fluid–solid and solid–solid phases. Numerous literature reports, pertaining to colloidal and similar systems, show that the phase diagram is sensitive to the attractive range of the potential [9–11]. When the interaction potential becomes short-ranged, the stable fluid–fluid phase transition disappears and only the solid–fluid coexistence curve is thermodynamically stable. As shown by simulation studies, the minimum range of attraction required for the fluid–fluid coexistence in aqueous protein or similar systems is about one sixth of the particle diameter [12]. For very short-ranged attractions, smaller than about one twentieth of the particle diameter, a stable isostructural solid–solid transition appears [13].

It has been observed that charged-stabilized colloidal suspensions can display interesting thermodynamic behavior such as liquid–vapor coexistence [14] and stable voids [3,15] etc. Such behaviors reveal an extraordinary cohesion phenomenon between like-charged macro-ions with screened electrostatic interactions. In those cases the relevant forces between particles can be well described with hard-core attractive Yukawa (HCAY) potential. Its interaction ranges can be varied from short range appropriate for modeling of colloidal suspensions [16,17], protein solutions [18] and fullerenes [19] to medium range, where it mimics the familiar

* Corresponding author.
E-mail address: jayantks@iitk.ac.in (J.K. Singh).

0009-2614/$ - see front matter © 2010 Elsevier B.V. All rights reserved.
doi:10.1016/j.cplett.2010.06.005

LJ potential [20] or to long-ranged potentials. Much attention has been paid in recent years to the HCAY potential model by its analytical tractability in the context of liquid state theories.

The liquid–vapor equilibrium of bulk phase HCAY fluids has been already estimated by computer simulation [21–23] and some theoretical efforts for these fluids have been done [24–26]. Despite the importance of the Yukawa model in relation to the adhesive hard sphere (AHS) potential [27–29], confining effects of surfaces with varying attraction and screening range have not been studied to make their connection to the detailed dependence of vapor–liquid phase diagram and critical properties of colloidal fluids. This has a practical importance in the field of nano structure formation, for example in processing of nanoparticles and evaporation-driven self-assembly, where nano-colloidal suspension interacts with each other. Hence, it is of significant interest to understand how the behavior of the colloid fluid phase is influenced by the nanoscopic confinement, where the interaction of confining surfaces with confined atoms or molecules is smeared by the presence of charged ions on the surface of the colloid. The non-monotonic behavior of critical temperature, T_{cp} have been studied in other model fluids in different confinements such as, square-well fluid in a cylindrical pore of varying wall-fluid interaction strength, ε_{wf}, which is reported by Zhang and Wang's study [30] using DFT calculations. Singh et al. [31,32] also reported a similar observation of the non-monotonic change in T_{cp} for square-well fluids in slit pores. In this current work, we address the effect of screening parameter along with the surface attraction of the Yukawa-modeled surfaces on the vapor–liquid phase behavior and critical properties of colloidal fluid and additionally, the 3D–2D crossover behavior of the colloidal fluid in the slit-pore-confined geometry. The rest of the Letter is organized as follows: in the next section, we briefly describe methods used for calculating the phase equilibria and critical properties by molecular simulation along with simulation details; the Section 3 presents results and discussion followed by the conclusion in the Section 4.

2. Potential model and simulation details

We have simulated the colloidal system in the grand canonical (GC) ensemble using transition matrix Monte Carlo (TMMC) technique [33], in order to locate the vapor–liquid phase equilibria of the slit-pore-confined system. The model potential for fluid–fluid and surface–fluid are represented by following expressions:

$$u_{ff}(r) = \begin{cases} \infty & \text{if } r < \sigma_{ff} \\ -\frac{\varepsilon_{ff}\sigma_{ff}}{r}\ \exp(-K_{pp}(r-\sigma_{ff})) & \text{if } r \geqslant \sigma_{ff} \end{cases} \quad (1)$$

$$u_{wf}(z) = \begin{cases} \infty & \text{if } z < \sigma_{wf} \\ \varepsilon_{wf}\ \exp(-K_{wp}(z-\sigma_{wf})) & \text{if } z\ \geqslant \sigma_{wf} \end{cases} \quad (2)$$

where, the set of parameters (i.e. ε_{ff}, σ_{ff} , K_{pp} and ε_{wf}, σ_{wf}, K_{wp}) represent the potential depth, the hard-core diameter and the interaction ranges of fluid–fluid and surface–fluid interactions, respectively. In this work ε_{ff} and σ_{ff} are taken as unity and σ_{wf} is a half of σ_{ff}. All quantities reported in this work are made non-dimensional using characteristic energy, ε_{ff}, and length scale, σ_{ff}. All simulations in this work are done at the fluid of a fixed $K_{pp} = 3$ and cut-off radius 4. Moreover, ε_{wf} is varied discretely from 1 to 4. Simulations are conducted in the GC ensemble, where the chemical potential μ, the volume V and the temperature T are kept constant, and the number of particles N and the energy U fluctuate. Detailed methodology is described in the earlier work [23]. In this work, the temperature, the pressure, the density are normalized with respect to simulation units, but expressed simply by T, ρ and P, respectively. Critical properties are estimated by using the coexistence data obtained via GC-TMMC and the least square fit of the following scaling law [33]:

$$\rho_l - \rho_v = C(1 - \frac{T}{T_C})^{\beta} \quad (3)$$

where, ρ_l, ρ_v, and T_C are coexistence liquid and vapor number densities, and critical temperature, respectively, and C and β are fitting parameters. The parameter β is also known as the order parameter critical exponent. However, in the current investigation we have not use mixed-field finite size scaling approach to evaluate the pore critical temperature, but a recent study using finite size scaling approach [34] for the estimation of critical point of Lennard–Jones fluid in hard slit pore confinement show similar behavior as reported in some other recent work [32,35] using the current technique. The critical temperature, T_C, estimated from Eq. (3) is used to calculate the critical density, ρ_c, from the least square fit of the following equation:

$$\frac{\rho_l + \rho_v}{2} = \rho_c + D(T - T_C) \quad (4)$$

where, D is a fitting parameter. Critical pressure, P_c, is calculated using the least square fitting of the saturation pressure data obtained from the GC-TMMC simulations to the following expression, which has a form similar to the Antoine equation:

$$\ln P_c = A - \frac{B}{T_c} \quad (5)$$

where, A and B are fitting parameters. The above empirical formula has been used to obtain the critical pressure for confined square-well fluids [32] and alkanes [36]. The saturated density profiles (i.e. perpendicular to the slit surface), ρ_z is obtained by recording $\rho(N, z)$ for each particle number sampled during GC-TMMC simulations. Coexistence density profiles are finally obtained using the following expression:

$$\rho(z)_{\text{vapor/liquid}} = \frac{\sum_{i\in\text{vapor/liquid}} \Pi_C(i)\rho(i,z)}{\sum_{i\in\text{vapor/liquid}} \Pi_C(i)} \quad (6)$$

where, Π_C is the coexistence probability density distribution obtained by applying the histogram reweighting technique [37] on the transition matrix data obtained from the GC-TMMC simulation.

GC-TMMC simulations are conducted with 30% displacement and 70% insertion/deletion moves. We use different numbers of particles for particular cases under consideration to keep optimal simulation environments; for phase coexistence calculation at various H and a fixed $K_{wp} = 1.8$ and $\varepsilon_{wf} = 2$, maximum number of particles are varied from around 800–6200, depending upon H. However, at a fixed $H = 8$ and $\varepsilon_{wf} = 4$, with various K_{wp}, maximum number of particles are varied from 800 to 2000 and for the hard-wall slit pore with $H = 8$, maximum number of particles are varied from around 800–2400. Four independent runs are conducted to obtain the statistical error in coexisting densities and critical properties. The errors in T_c, ρ_c and P_c for the studied slit pore geometries are found to be less than 0.05%, 0.02% and 0.1%, respectively.

3. Results and discussion

3.1. Vapor–liquid phase equilibria and critical properties under confinement

In Fig. 1, we have shown the variation of surface–fluid potential energy, U_{wf}, vs. distance, z, of colloidal molecules with a typical surface well depths, $\varepsilon_{wf} = 4$ and for varying ranges of surface–fluid interactions, K_{wp}. Increasing K_{wp} diminishes the effective attraction of the surface-colloidal molecules and the behavior approaches to

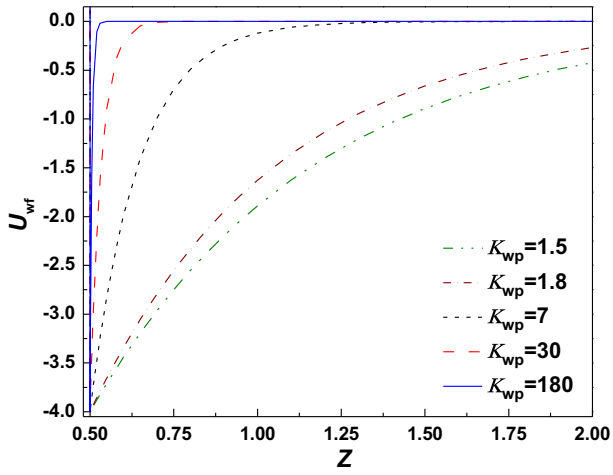

Fig. 1. Surface–fluid potential energies, U_{wf}, are shown for variable surface–fluid interaction range, K_{wp}, with a typical well-depth of the surface–fluid attraction, $\varepsilon_{wf} = 4$.

the sticky-wall behavior as it becomes sufficiently large. At infinitely large K_{wp} the surface behaves as hard-wall.

Fig. 2 illustrates the vapor–liquid phase coexistence envelopes for a typical surface well-depths, $\varepsilon_{wf} = 4$ for varying K_{wp} in comparison with the hard wall, $\varepsilon_{wf} = 0$. Similar behavior of vapor–liquid coexistence envelope is observed with other values of $\varepsilon_{wf} = 1$ and 2. However, for the sake of clarity we have shown the coexistence envelope only for $\varepsilon_{wf} = 4$. It is observed that at a smaller well-depth, $\varepsilon_{wf} = 1$, with increase in the interaction range, i.e. decrease in K_{wp}, critical temperature and density increases (figure not shown). However, with such observation, an important question arise that, will these critical properties increase, decrease or remain constant with the surface interaction range? Nevertheless, the critical temperature under the confinement cannot exceed the bulk critical temperature, hence it is expected that with further increase in the interaction range the critical temperature will either approach the bulk value or bear a non-monotonic behavior. To realize this interesting behavior of critical properties, we have

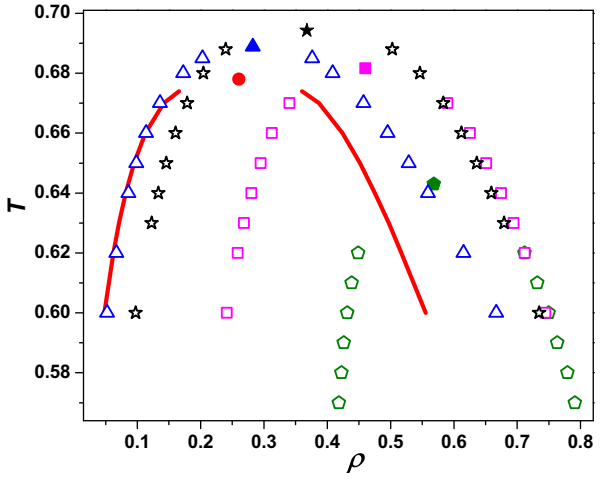

Fig. 2. Temperature–density vapor–liquid coexistence curve for a colloidal fluid in the slit pore confinement of pore width $H = 8$, and at a typical wall–fluid interaction well depth, $\varepsilon_{wf} = 4$ with variable interaction ranges, K_{wp}, are shown. Solid curves represent the hard-wall coexistence densities with the symbol filled circle as the critical point. Open and filled symbols represent the coexistence densities and the critical points respectively. Symbols triangle, star, square and pentagon represent the case with $K_{wp} = 180$, 30, 7 and 1.8, respectively.

run some simulations with comparatively higher well depths, $\varepsilon_{wf} = 2$ and 4. For a complete view of the phenomenon a hard-wall confined colloidal system is also investigated. As the surface becomes comparatively attractive, $\varepsilon_{wf} = 4$ and $K_{wp} = 180$ i.e., sticky-wall, as compared to the hard-wall, critical temperature and density increase, and similar behavior is observed with the other studied cases of $\varepsilon_{wf} = 1$ and 2. Moreover, with further increase in the interaction range, (i.e. from $K_{wp} = 180$ to 30) critical point monotonically increases. Interestingly, with further increase in the interaction range to $K_{wp} = 7$, it is observed that critical temperature decreases, however, critical density retains its increasing monotonic nature. The decrease of the critical temperature and the increase of the critical density are continued with further increase in the interaction range to $K_{wp} = 1.8$, as depicted in Fig. 2.

To elucidate the non-monotonic trend of the critical temperature with the increase in the effective interaction range, some more insightful discussions are required. From the scaling law point of view [33], critical temperature and density depend on the relative width of the coexistence envelope. From Fig. 2, it is clear that in comparison with hard-wall ($K_{wp} \to \infty$, or $\varepsilon_{wf} = 0$) slit pore, the width of the coexistence envelope comparatively increases with increase in the interaction range from $K_{wp} = \infty$ to 180. The change in the saturated vapor densities is insignificant with the change in $K_{wp} = \infty$–180, yet the corresponding change in the liquid branch is significant which consequently resulted in the increase of critical temperature and density. In the comparison between $K_{wp} = 180$ and 30, the coexistence envelope in Fig. 2 shows that at $K_{wp} = 30$, both vapor and liquid density branches shift toward higher value but the comparative shift of the liquid density branch is higher, which in turn resulted in a wider coexistence envelope at $K_{wp} = 30$ as compared to 180. This resulted in increases of T_{cp} and ρ_{cp}. With further increase in the interaction range from $K_{wp} = 30$ to 7, the vapor density branch shows a significant increase but the shift in the liquid density branch is comparatively insignificant. These comparatively opposite changes cause the decrease of the coexistence envelope width, hence the decrease of T_{cp}. Furthe increase in the interaction range from $K_{wp} = 7$ to 1.8, led to an insignificant change in the liquid density branch; on the other hand, vapor density branch shifts toward a higher value and resulting in the decrease of the coexistence envelope width and thus T_{cp}. More insights are required to explain the interesting phenomenon, which is the non-monotonic behavior of the critical temperature of colloidal-like confined fluids, in particular with a fixed interaction well-depth but varied interaction range. While converse examples are emphasized in the introduction section, detailed investigations on the local vapor and liquid phase densities at different K_{wp}'s must be performed to validate the average coexistence densities of vapor and liquid phases observed in the phase coexistence envelope of Fig. 2.

In Fig. 3a and b local z-density profile of coexisting vapor and liquid phases are shown respectively, for a typical case $T = 0.6$. To observe the local structural behavior of the confined fluid near the surface, local z-density profile of remaining slit width i.e., from $H/2$ to H (z-direction) is not shown in (a) and (b) as the behavior is same as in the first half of the pore. Fig. 3a shows that with increase in the attraction range, vapor like phase become more and more structured and intensity as well as width of the density peak increases for the studied cases, $K_{wp} = 180$ to 7. However, when attraction range becomes sufficiently large as is the case with $K_{wp} = 1.8$, intensity of the peaks nearest to either of the surfaces diminishes at the expense of increase in peak width as can be seen from Fig. 3b. Moreover, Intensity of the other peaks with $K_{wp} = 1.8$ is larger as compared to the peaks of lower attraction ranges. This in turn resulted in increased average density of vapor phase as compared to others. On the other hand, local structural behavior of liquid like phase is more interesting than the vapor like phase. It is

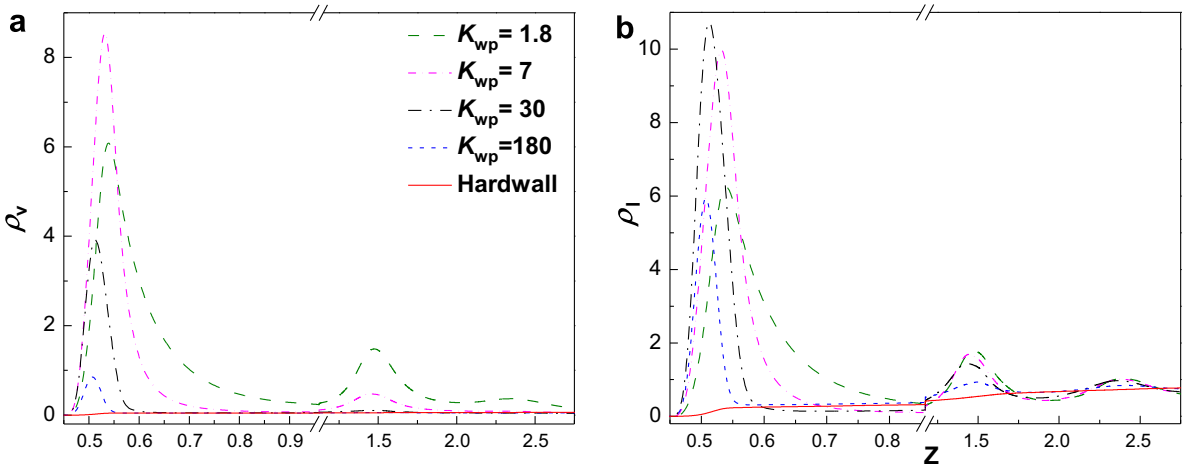

Fig. 3. Local z-density profiles of vapor and liquid phase are shown in (a) and (b) respectively for a model colloidal fluid with $\varepsilon_{wf} = 4$, at $T = 0.6$, in a slit pore with width $H = 8$ for various values of K_{wp}. In addition, hard-wall case is also included. For the sake of clear visibility of the peak behaviors, remaining other local z-density data points are not shown in the plots. In (b), curves have the same meaning as in (a).

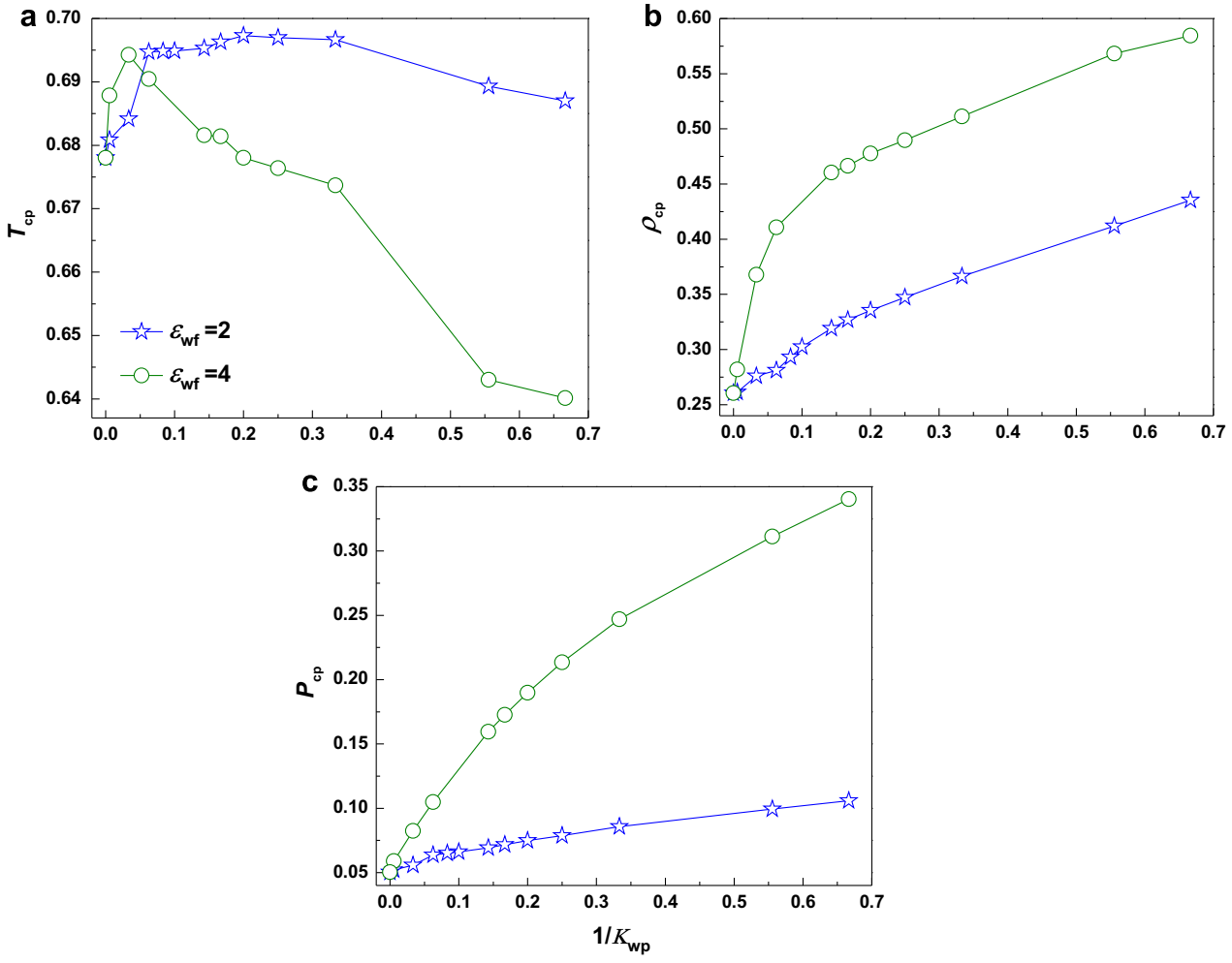

Fig. 4. The dependences of T_{cp}, ρ_{cp} and P_{cp} on the inverse of the screening parameter, K_{wp}, are plotted for two surface well-depths, $\varepsilon_{wf} = 2$ and 4, are shown in (a), (b) and (c), respectively.

shown in Fig. 3b that with increase in attraction range, intensity and width of the peaks nearest to either of the pore surfaces increases until $K_{wp} = 30$ (contrary to the vapor phase where the increasing trend is until $K_{wp} = 7$) and then intensity of the peaks nearest to the surfaces diminishes from $K_{wp} = 7$ until $K_{wp} = 1.8$, at the expense of increase in peak width. Moreover, qualitatively

intensity of other peaks follow similar trend as the vapor phase peaks. Thus the two opposing behavior, i.e., decrease in intensity of the peak and increase of peak width resulted in insignificant change in average liquid phase densities for the case of $K_{wp} = 30$, 7 and 1.8, in spite of increase in the surface–fluid attraction range as can be seen from the Fig. 1 of surface–fluid potential plot. Coexistence phase diagram of Fig. 2 shows insignificant change in liquid phase densities for $K_{wp} = 30$, 7 and 1.8. With the local z-density profiles of various K_{wp}, at a typical case of $T = 0.6$, it has been validated that the average values of fluid coexistence densities observed in Fig. 2 are reasonable and hence the coexistence envelope. This in turn resulted in the non-monotonic trend of critical temperature with change in K_{wp}.

In Fig. 4a–c, T_{cp}, ρ_{cp} and P_{cp} are shown respectively, with two typical cases of surface attraction well-depths, $\varepsilon_{wf} = 2$ and 4 with a fixed $H = 8$ and various K_{wp}'s. Fig. 4a shows that as the interaction range increases, T_{cp} follows non-monotonic paths depending the surface well-depth, ε_{wf}. At a stronger surface field, $\varepsilon_{wf} = 4$, the maximum in T_{cp} is observed at a comparatively smaller interaction range; but at a weaker surface field, $\varepsilon_{wf} = 2$, the maximum of T_{cp} occurs at larger interaction range. Moreover, at sticky-wall limit, critical properties with the studied smaller ε_{wf}, approach to the hard-wall value prior to that seen for relatively larger ε_{wf}, as expected. Interestingly, there only exist one maxima of T_{cp} for each ε_{wf} studied for $H = 8$. Contrary to the non-monotonic trend of T_{cp}, we observed monotonically increasing trends in ρ_{cp} and P_{cp} as shown in Fig. 4b and c, for all cases under consideration, as the interaction range increases.

3.2. Crossover from 3D to 2D behavior

In this work, the critical temperature is calculated by rectilinear diameter approach as mentioned in Section 2. Fig. 5, for a typical case of colloidal fluid at $\varepsilon_{wf} = 2$ and $K_{wp} = 1.8$, presents the variation of the pore critical temperature, T_{cp}, reduced by 3D bulk value, i.e. T_{cp}/T_{cb}, (where, $T_{cb} = 0.722(1)$ is the bulk critical temperature predicted in the earlier investigation [23]) versus the slit width, H. It has shown that T_{cp}/T_{cb} changes monotonically with H and slowly approaches 1 for H much larger than 20. In the current investigation, we have studied the 3D to 2D crossover behavior of the confined colloidal fluid as shown in the inset of Fig. 5. Fisher and Nakanishi [38] with the help of scaling arguments showed that the decrease in the critical temperature in larger pores should obey the relation, $(T_{cb}-T_{cp})/T_{cb} = kH^{-1/\nu}$, where ν is the critical exponent for the correlation length and k is a proportionality constant. To account for the strongly adsorbed layer on pore walls it is necessary to replace the true pore width, H, by a modified pore width, $H_{eff} = H-t$, where t represents the effective layering thickness. Using Ising 3D (bulk) correlation length critical exponent $\nu(3D) = 0.63$, and Ising 2D correlation length critical exponent[39], $\nu = 1$, we have evaluated the effective layering thickness, t, of the adsorbed layer in the slit pore by fitting the logarithmic form of the relation, $(T_{cb}-T_{cp})/T_{cb} = k(H-t)^{-1/\nu}$. We observed that for larger pore width t is insignificant irrespective of the surface attraction. However, for smaller pores it is appreciable. In the current investigation with a typical case of $\varepsilon_{wf} = 2$, $K_{wp} = 1.8$, and $K_{pp} = 3$, a layering thickness is observed to be around 1.4 in the smaller pore regime. However, in the larger pore regime the layering thickness of around 2.76×10^{-14} is extremely small. In the inset of Fig. 5, the relative critical temperature, $(T_{cb}-T_{cp})/T_{cb}$, is plotted as a function of the effective slit width, H_{eff}, on a log–log scale for a typical case. It is evident from inset Fig. 5 that the crossover from 3D to 2D is at around $H \sim 14$ molecular diameters for the studied Yukawa system in this work.

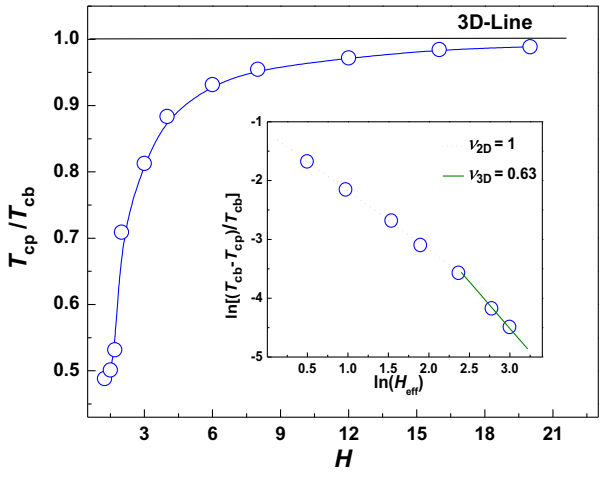

Fig. 5. Dependence of pore critical temperatures, T_{cp} (reduced by the corresponding bulk value, T_{cb}) of a colloidal fluid on the slit width H and its approach to 3D value is shown. In inset, crossover from 3D to 2D behavior is shown. All the simulation run are carried out with a fixed surface attraction well depth, $\varepsilon_{wf} = 2$ and surface interaction range $K_{wp} = 1.8$. Symbol circle represents the simulation data points.

4. Conclusions

We have reported a simulation study aimed at evaluating the dependence of the surface–fluid interaction well-depth and the interaction range on the vapor–liquid coexistence and critical properties of confined colloidal fluids. These investigations suggest that having a fixed fluid–fluid interaction well-depth, the surface interaction range plays an important role on the non-monotonic behavior of the critical temperature of confined colloidal fluids. Starting from extremely small interaction range, $K_{wp} = 180$, to the larger interaction range, $K_{wp} = 1.5$, the critical temperature shows a non-monotonic path, irrespective of the surface interaction well-depth, ε_{wf}, studied in the current work. On the other hand, critical density and pressure display a monotonically increasing nature with the increase in the surface interaction range. In the current work, we have also studied the 3D to 2D crossover behavior of colloidal fluid. We observed that crossover behavior occurs at around 14 molecular diameters for the considered Yukawa based model colloidal system in the current work.

Acknowledgment

This work was supported by the Department of Science and Technology, Govt. of India. (Grant No: SR/S3/CE/061/2009).

References

[1] G. Pellicane, D. Costa, C. Caccamo, Phys.: Condens. Matter 16 (2004) 4923.
[2] D. Rosenbaum, P.C. Zamora, C.F. Zukoski, Phys. Rev. Lett. 76 (1996) 150.
[3] K. Ito, H. Yoshida, N. Ise, Science 263 (1994) 66.
[4] A.E. Larsen, D.G. Grier, Nature 385 (1997) 230.
[5] B. Zoetekouw, Rev. Lett. 97 (2006) 258302.
[6] S.H.L. Klapp, S. Qu, R.V. Klitzing, J. Phys. Chem. B 111 (2007) 1296.
[7] S.H.L. Klapp, Y. Zeng, D. Qu, R.V. Klitzing, Phys. Rev. Lett. 100 (2008) 118303.
[8] V.J. Anderson, H.N.W. Lekkerkerker, Nature 416 (2002) 811.
[9] F. Renth, W.C.K. Poon, R.M.L. Poon Evans, Phys. Rev. E 64 (2001) 031402.
[10] J.Z. Wu, J.M. Prausnitz, Fluid Phase Equilib. 194–197 (2002).
[11] F.W. Tavares, S.I. Sandler, AIChE J. 43 (1997) 218.
[12] M. Dijkstra, Rev. E 66 (2002) 021402.
[13] P. Bolhuis, M. Hagen, D. Frenkel, Phys. Rev. E 50 (1994) 4880.
[14] B.V.R. Tata, M. Rajalakshmi, A.K. Arora, Phys. Rev. Lett. 69 (1992) 3778.
[15] N. Ise, T. Konishi, B.V.R. Tata, Langmuir 15 (1999) 4176.
[16] C. Caccamo, G. Pellicane, D. Costa, Phys.: Condens. Matter 12 (2000) A437.
[17] T. Kristóf, D. Boda, J. Liszi, D. Henderson, E. Carlson, Mol. Phys. 101 (2003) 1611.
[18] W. Olivares, L. Degreve, J.C. Villegas, M. Lozada-Cassou, Phys. Rev. E 65 (2002) 061702.

[19] C. Caccamo, G. Pellicane, D. Costa, D. Pini, G. Stell, Phys. Rev. E 60 (1999) 5533.
[20] D. Pini, G. Stell, N.B. Wilding, J. Chem. Phys. 115 (2001) 2702.
[21] D. Pini, G. Stell, N.B. Wilding, Mol. Phys. 95 (1998) 483.
[22] M.H.J. Hagen, D. Frenkel, J. Chem. Phys. 101 (1994) 4093.
[23] J.K. Singh, Mol. Simul. 35 (2009) 880.
[24] E.B. El Mendoub, J.F. Wax, N. Jakse, Phys. Rev. E 74 (2006) 052501.
[25] P. Paricaud, Chem. Phys. 124 (2006) 154505.
[26] R. Tuinier, G.J. Fleer, J. Phys. Chem. B 110 (2006) 20540.
[27] P. Prinsen, T. Odijk, J. Chem. Phys. 125 (2006) 074903.
[28] M.L. Broide, T.M. Tominc, M.D. Saxowsky, Phys. Rev. E 53 (1996) 6325.
[29] J. Largo, M.A. Miller, F. Sciortino, J. Chem. Phys. 128 (2008) 134513.
[30] X. Zhang, W. Wang, Phys. Rev. E 74 (2006) 062601.
[31] J.K. Singh, S.K. Kwak, J. Chem. Phys. 126 (2007) 24702.
[32] S.K. Singh, A.K. Saha, J.K. Singh, J. Phys. Chem. B 114 (2010) 4283.
[33] J.R. Errington, Chem. Phys. 118 (2003) 9915.
[34] Y. Liu, A.Z. Panagiotopoulos, P.G. Debenedetti, J. Chem. Phys. 132 (2010) 144107.
[35] S. Jana, J.K. Singh, S.K. Kwak, J. Chem. Phys. 130 (2009) 214707.
[36] S.K. Singh, A. Sinha, G. Deo, J.K. Singh, J. Phys. Chem. C 113 (2009) 7170.
[37] A.M. Ferrenberg, R.H. Swendsen, Phys. Rev. Lett. 61 (1988) 2635.
[38] M. Fisher, H. Nakanishi, J. Chem. Phys. 75 (1981) 5857.
[39] R. Evans, Chem. Phys. 84 (1986) 2376.